The NAMI A – human ferritin system: a biophysical characterization†

Silvia Ciambellotti, [a,b] Alessandro Pratesi, [c] Mirko Severi, [b] Giarita Ferraro, [d] Enzo Alessio, [e] Antonello Merlino *[d] and Luigi Messori *[c]

The reaction of the antimetastatic ruthenium(III) drug NAMI A with human H-chain ferritin (HuHf) was investigated through a variety of biophysical methods. We observed that the addition of HuHf to NAMI A solutions significantly increases the rate of spontaneous NAMI A hydrolysis suggesting the occurrence of a direct metallodrug–protein interaction. The resulting hydrolyzed Ru species binds the protein mostly forming a relatively tight 1 : 1 ruthenium/ferritin (subunit) adduct that was then separated and characterized. Notably, this adduct shows a characteristic CD spectrum in the visible region, which is diagnostic of the existence of at least one protein bound ruthenium center. The crystal structure of this NAMI A/HuHf adduct was subsequently solved at 1.58 Å resolution; clear evidence is given for the selective binding of a single Ru ion to His105 of each subunit with concomitant release of all other original Ru ligands in agreement with previous observations. We also noted that NAMI A produces a partial inhibition of HuHf ferroxidase activity. The implications of the above results are discussed.

Accepted 22nd July 2018

Introduction

Ruthenium-based compounds have been extensively studied, during the past two decades, as promising anticancer agents and as an alternative to platinum-based drugs for cancer treatment.[1,2] Among them, imidazolium *trans*-imidazoledimethylsulfoxide-tetrachlororuthenate, ImH[*trans*-$RuCl_4$(DMSO)Im] (NAMI A hereafter, Scheme 1) is a well-known ruthenium(III) compound showing attractive anticancer properties. NAMI A is commonly considered as a scarcely cytotoxic agent but manifests relevant antimetastatic properties both *in vitro* and *in vivo*,[3–5] as described in detail by G. Sava and co-workers through many research articles.[6,7] Owing to its favourable pharmacological profile, NAMI A has been eventually admitted to phase II clinical trials.[8]

As NAMI A is quite a reactive species that may undergo progressive and relatively rapid transformations – both in blood and in tissues – before entering cells,[3] we wondered whether it is possible to prepare NAMI A/protein adducts that might protect the drug from these transformation reactions for a longer time and/or improve its cellular uptake and/or pharmacological profile.

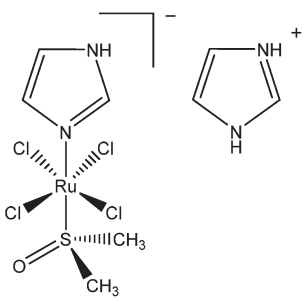

Scheme 1 ImH[*trans*-$RuCl_4$(DMSO)Im], NAMI A.

To this end, we decided to study the reaction of NAMI A with human ferritin. Ferritin is one of the main players in iron metabolism.[9,10] The biological role of ferritin is the storage of ferric ions within its cavity in the form of a hydrated ferric oxide biomineral, thus preventing the uncontrolled accumulation of toxic iron species inside cells.

Ferritins are constituted by 24 subunits that self-assemble giving rise to an almost spherical nanocage. The ferritin cage has 2,3,4-fold symmetry (*C*2, *C*3 and *C*4 symmetry axes). The exterior and interior of the cage are connected *via* channels along *C*3 and *C*4 symmetry axes at subunit junctions.[11]

[a]*Magnetic Resonance Center (CERM), University of Florence, 50019 Sesto Fiorentino, Italy*
[b]*Department of Chemistry, University of Florence, 50019 Sesto Fiorentino, Italy*
[c]*Laboratory of Metals in Medicine (MetMed), Department of Chemistry, University of Florence, 50019 Sesto Fiorentino, Italy. E-mail: luigi.messori@unifi.it*
[d]*Department of Chemical Sciences, University of Naples Federico II, Complesso Universitario di Monte Sant'Angelo, 80126 Napoli, Italy. E-mail: antonello.merlino@unina.it*
[e]*Department of Chemical and Pharmaceutical Sciences, University of Trieste, 34127 Trieste, Italy*

Mammalian ferritins are formed by two types of subunits: heavy (H) and light (L) chains, in a tissue specific ratio, according to cell needs. All subunits share a common fold: a bundle of four antiparallel helices (H1–H4), a fifth short helix (H5) and a long solvent-exposed loop connecting H2 and H3. The H-chain contains a binuclear ferroxidase centre that catalyses iron(II) oxidation. This antioxidant activity consumes iron(II) and dioxygen or hydrogen peroxide, the reagents that produce toxic free radicals in the Fenton reaction. The ferric products that form at the ferroxidase centre are the precursors of the biomineral. In contrast, the L-chains lack enzymatic activity; yet, they are able to store iron as a caged biomineral, although biomineralization proceeds at a slower rate. The L-chain contains a large number of carboxylate groups lining the ferritin cavity and binding an iron cluster, recently proposed as the nucleation seed for biomineral growth.[12]

In recent times, ferritin has been proposed as a drug delivery system[13] since cells can recognize and incorporate exogenous ferritin using specific receptors. In particular, H-richer ferritins are recognized by TfR1 (transferrin receptor 1)[14] while L-richer ferritins by SCARA5 (scavenger receptor class A type 5),[15] both overexpressed in specific tumor cells.[16,17]

Due to its peculiar molecular architecture, ferritin has the unique possibility of encapsulating a large number of drug molecules inside its cavity. Drug encapsulated ferritin systems have been generally obtained using internalization protocols that are based on cage disassembly/reassembly procedures, which allow the trapping of the drug inside the cage.[18] Using these protocols, several molecules have been encapsulated within the ferritin nanocages, including cisplatin,[19,20] carboplatin,[21] oxaliplatin,[22] ruthenium[23,24] and gold-based drugs.[25,26] Recently, it has been shown that the loading of drugs within the ferritin nanocage can be obtained without disassembling the ferritin cage under harsh pH conditions.[27] Alternatively, ferritin may behave as a drug carrier by the reversible binding of drug molecules on its external surface. In this context, we have shown that it is possible to obtain a 1 : 1 complex between cisplatin and each H-chain subunit of human homopolymeric ferritin (HuHf), without using encapsulation protocols.[28]

Here, we investigate the interactions of NAMI A with HuHf to establish whether it is possible to prepare NAMI A/ferritin adducts with improved pharmacological properties. NAMI A was incubated with HuHf and the resulting adducts characterized from the biochemical and biophysical point of view. We noted that a predominant 1 : 1 Ru/ferritin subunit adduct is formed. Notably, the crystal structure of the NAMI A/HuHf adduct could be solved for the first time, allowing the identification of a single ruthenium binding site per subunit, located at the side chain of His105, which is exposed to the bulk solvent. In this crystal structure the ruthenium centre of NAMI A, once bound to the protein, has lost all its original ligands. Moreover, as ruthenium(III) ions (originating from NAMI A degradation) mimic quite closely iron(III) ions, we decided to explore whether NAMI A does inhibit to some extent the physiological function of ferritin.

Experimental

Protein expression and purification

Gene encoding HuHf subcloned in the pET-9a vector was transformed into *E. coli* BL21(DE3) pLysS competent cells. Bacteria were cultured in a rich medium (Luria Bertani broth) containing 50 mg L^{-1} of kanamycin and 34 mg L^{-1} of chloramphenicol at 37 °C. HuHf was produced and purified as previously described.[29,30] Briefly, when $A_{600\ nm}$ reached 0.6–0.8, the over-expression of HuHf was induced with 1 mM isopropyl β-D-1-thiogalactopyranoside (IPTG). The cells were harvested (7500 rpm for 15 minutes) and resuspended in 20 mM Tris-HCl buffer, pH 7.5. Lysis of cells was performed with sonication. The crude lysate was clarified with ultra-centrifugation (40 000 rpm for 40 minutes), and the soluble fraction was heated at 65 °C for 15 minutes to precipitate undesirable proteins (40 000 rpm for 15 minutes). Subsequently, the supernatant was dialyzed against 20 mM Tris-HCl pH 7.5 buffer and loaded into an anionic exchange column with a Q-Sepharose Fast Flow resin (GE Healthcare) to elute HuHf with a linear NaCl gradient (0 to 1 M) in 20 mM Tris-HCl, pH 7.5. Next, fractions with ferritin (identified with SDS-PAGE analysis) were pooled and further purified with size exclusion chromatography (HiLoad 16/60 Superdex 200 column, GE Healthcare). Iron and other metal ions were removed in four dialysis steps using 20 mM Tris-HCl, 3 mM EDTA, ammonium thioglycolate (1 : 400), and pH 7.5 buffer, to reduce and chelate the iron, followed by four dialysis steps against 20 mM Tris-HCl pH 7.5 buffer.

Spectrophotometric studies

HuHf (50 μM in subunits) was incubated with freshly prepared solutions of NAMI A at different molar ratios (1 : 2, 1 : 4 and 1 : 8) in phosphate buffer (50 mM sodium phosphate, 100 mM NaCl, pH 7.4). NAMI A was synthesized as previously described.[31] The hydrolysis experiments, both in the presence of the protein or with NAMI A alone, were monitored spectrophotometrically at room temperature over 24 hours. The electronic spectra were acquired with a Varian Cary 50 Bio UV-vis spectrophotometer using a general protocol previously developed in our lab.[32]

Circular dichroism analysis

The formation of NAMI A/protein adducts was assessed with circular dichroism in 50 mM sodium phosphate, 100 mM NaCl, pH 7.4. Spectra were registered using a Jasco J-810 spectropolarimeter. Spectra in the far UV region (190–250 nm at 10 μM HuHf in subunits) and in the UV-visible region between 300 and 700 nm (4 mM HuHf in subunits) were acquired on the ultra-filtered samples of apo HuHf and pre-incubated HuHf with increasing amounts of NAMI A for 24 h (from 2 to 8 NAMI A equivalents in the former analysis and till 2 equivalents in the latter). The mean of 10 accumulations was reported and calculated by the subtraction of the buffer spectrum. The CD data were registered using a scanning speed set at 100 nm min^{-1} and a bandwidth and data pitch of 0.5–1 nm;

temperature was maintained constant at 25 °C using the Jasco Peltier apparatus.

Enzymatic activity measurements

Single turnover oxidoreductase kinetics (2 Fe^{2+} ions per subunit) was monitored on HuHf. Changes in absorbance at 650 nm (diferric-peroxo or DFP) or at 350 nm (diferric-oxo/hydroxo species; DFO(H)) were acquired after rapid mixing (<10 ms) of equal volumes of 100 μM HuHf as subunit (native or ruthenated ferritin incubated with 2 NAMI A molecules per protein monomer for 24 h) in 200 mM 3-(*N*-morpholino)propanesulfonic acid (MOPS), 200 mM NaCl, pH 7.0, with freshly prepared solutions of 200 μM ferrous sulphate in 1 mM HCl, in a UV-visible, stopped-flow spectrophotometer (SX.18MV stopped-flow reaction analyser, Applied Photophysics). The NAMI A incubation with HuHf was performed in the classical phosphate buffer; then the sample was loaded into a PD-10 desalting column (GE Healthcare) to remove the unbound Ru species and for buffer exchange into 200 mM MOPS and 200 mM NaCl, pH 7. The final sample concentration was determined using the Bradford assay. Routinely, 4000 data points were collected during the first 5 s. Initial rates of DFP and DFO(H) species formation were determined using the data from three independent analyses through the linear fitting of the initial phases of absorbance changes at 650 and 350 nm traces (0.01–0.03 s).

High-resolution X-ray crystallography

Crystals of HuHf were grown at 293 K using the hanging drop vapour diffusion method, using protein concentration = 20 mg mL^{-1} and 2.0 M $MgCl_2$, 0.1 M bicine at pH 9.0 as a reservoir. Crystals of NAMI A/HuHf were obtained by a soaking procedure,[33] as previously done to obtain the adduct formed in the reaction between the same protein and cisplatin.[28] 1 μL of NAMI A, dissolved in water at a concentration equal to 20 mM, was mixed with 1 μL of the reservoir and then 1 μL of this solution was added to the droplet containing HuHf crystals. Incubation time: 5 days. The crystals rapidly turn their colour to red/brown with time (Fig. 1).

The X-ray diffraction data on these crystals, cryoprotected using a solution obtained by the addition of 25% (v/v) (final concentration) glycerol to the reservoir, were collected at 1.58 Å resolution on the beamline ID30A at the European synchrotron radiation facility (ESRF), Grenoble, France. The data were indexed and scaled with iMosflm.[34] Data collection statistics of the best NAMI A/HuHf crystal are reported in Table 1. The structure was solved by molecular replacement using the program Phaser[35] and employing the structure of the native protein, without solvent, deposited under the accession code 5N27, as the search model.[28] Coordinates were refined using Refmac5[36] and model building was carried out using Coot.[37] Most of the model is revealed to have very good electron density. The final structure refines to an R_{factor} of 0.142 (R_{free} 0.183). Refinement statistics are summarized in Table 1. Validation was performed using PROCHECK.[38] The figures were obtained using Pymol.[39] Coordinates were deposited in the Protein Data Bank[40] under the accession code 6FTV.

Fig. 1 Crystals of HuHf before (first image) and after soaking in the presence of NAMI A.

Table 1 Data collection and refinement statistics

Parameter	HuHf-NAMI A
Diffraction source	ESRF synchrotron, Grenoble, France
Wavelength (Å)	0.9677
Temperature (K)	100
Space group	F432
$a = b = c$ (Å)	182.38
Resolution range (Å)	105.30–1.58 (1.61–1.58)
Total no. of reflections	270 843
No. of unique reflections	35 972
Completeness (%)	99.7 (100)
$CC_{1/2}$	0.996 (0.536)
Multiplicity	7.5 (7.8)
$\langle I/\sigma(I)\rangle$	14.5 (2.0)
$R_{merge.}$	0.068 (0.971)
Overall *B* factor from the Wilson plot (Å^2)	31.0
Resolution range (Å)	105.30–1.58
No. of reflections, working set	34 116
No. of reflections, test set	1842
Final R_{cryst} (%)	14.2
Final R_{free} (%)	18.3
No. of non-H atoms	1791
R.m.s. deviations from the ideal geometry	
Bonds (Å)	0.023
Angles (°)	2.13
Average *B* factors (Å^2)	25.19
Occupancy of Ru centres	0.25, 0.35
B-Factors of Ru centres	69.2, 44.8
Ramachandran plot[a]	
Most favoured (%)	98.5
Allowed (%)	1.5

Values in parentheses are for the outer shell. [a] Calculated for non-glycine and non-proline residues using Coot.

ICP-AES analysis

The ICP-AES data were collected following a well-established protocol[41] on the NAMI A/HuHf adduct, prepared incubating for 24 h at r.t. the protein in the presence of NAMI A in 1 : 2, 1 : 4 and 1 : 8 protein-to-metal ratios in phosphate buffer (50 mM sodium phosphate, 100 mM NaCl, pH 7.4). Successively, the metallated proteins were isolated using a centrifugal filter device with a cut-off membrane of 10 kDa and washed several times with the same phosphate buffer. The final metal/protein adducts were recovered by spinning the filters upside down at 3500 rpm for 3 min with 200 μL of the

phosphate buffer. The samples were mineralized in a thermoreactor at 80 °C for 8 h with 1.0 mL of HCl 30% Suprapur grade. After that, the samples were diluted exactly to 6 mL with ultrapure water (≤18 MΩ). The determination of ruthenium content under these solutions was performed using a Varian 720-ES Inductively Coupled Plasma Atomic Emission Spectrometer (ICP-AES). The calibration curve of ruthenium was obtained using known concentrations of a Ru ICP standard solution purchased from Sigma-Aldrich. Moreover, each sample was spiked with 1 ppm of Ge used as an internal standard. The wavelength used for Ru determination was 267.876 nm whereas for Ge the line at 209.426 nm was used. The operating conditions were optimized to obtain maximum signal intensity and, between each sample, a rinse solution containing 1.0 mL of HCl 30% Suprapur grade and 5.0 mL of ultrapure water was used to avoid any "memory effect". The final protein concentration was determined on the recovered protein/metal adduct using the Bradford assay and referred to the monomeric protein.

Results and discussion

The reaction of NAMI A with ferritin: spectrophotometric profiles

Owing to its characteristic absorption bands in the UV-visible region, the solution behaviour of NAMI A can be followed spectrophotometrically quite straightforwardly.[42] In particular, we analysed the effect of HuHf addition on the time-dependent spectral evolution of a NAMI A solution, in phosphate buffer (50 mM sodium phosphate, 100 mM NaCl, pH 7.4) over 24 hours of incubation, at room temperature. The spectral profile of NAMI A alone is characterized by an absorption band centered at 390 nm that progressively disappears, meaning that the first chloride ligand is lost and replaced by a water molecule, in agreement with the literature data.[31,43,44] At this point, an intense absorption band at 340 nm appears that subsequently decreases when the second chloride ligand is released and the second aquation step occurs (Fig. 2A, left panel).[42]

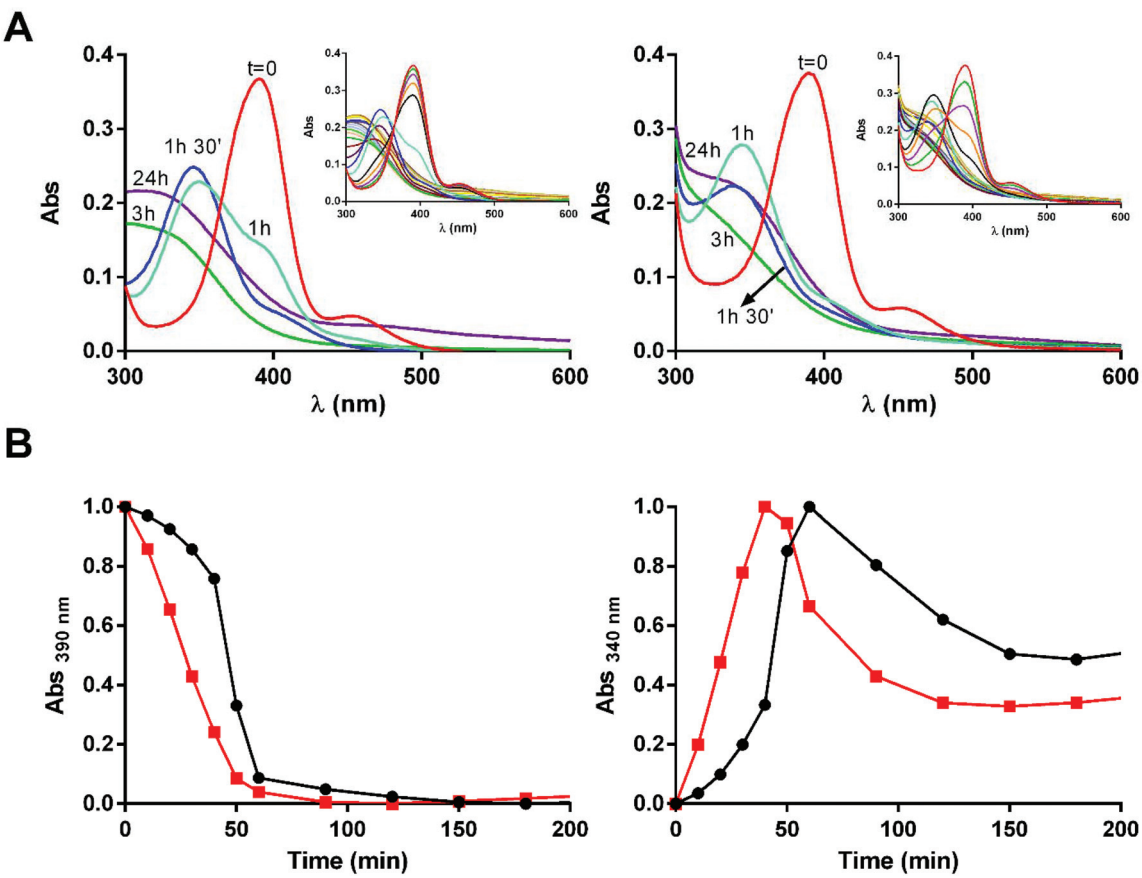

Fig. 2 Spectral evolution of NAMI A alone and in the presence of HuHf. (A) Time-course UV-vis spectra of the hydrolysis of NAMI A alone (100 μM solution) dissolved in 50 mM sodium phosphate and 100 mM NaCl, pH 7.4, on the left and in the presence of HuHf (50 μM in subunits, 1 : 2 HuHf : Ru ratio) on the right. The complete series of spectra, shown in the insets, was recorded over 24 hours at room temperature according to the following scheme: one spectrum every 10 minutes in the first hour, every 30 minutes till 6 hours and every 3 hours to the end of the acquisition. (B) The left panel shows the decrease in absorbance at 390 nm over time (peculiar evolution indicating the first chloride ligand loss and its replacement by a water molecule), while the right panel represents the increase in absorbance at 340 nm and its progressive decrease (the second chloride ligand is lost followed by the second aquation) in the first 200 min. The absorption behaviours of NAMI A alone (black curve) and in the presence of ferritin (red curve) are reported.

Then, the formation of a new maximum at 325 nm and a general increase of the background absorption attributable to the formation of ruthenium oligomers take place. A similar time-dependent profile is observed in the spectra acquired in the presence of ferritin (Fig. 2A, right panel); in this case, the hydrolysis of NAMI A occurs slightly faster than for NAMI A alone (Fig. 2B). This rate increase may be tentatively attributed to the occurrence of weak non-covalent interactions between the surface of the protein and the tetrachlororuthenate species, as already observed for the interaction of NAMI A with BSA.[44] Moreover, in the presence of HuHf, a colour shift of the solution from pale yellow, once NAMI A was added, to red/brown, at the end of the exposure, was observed.

Recovery and characterization of the NAMI A/HuHf adduct

At the end of the process, the samples were extensively ultrafiltered to remove excess of the non-reacted Ru compound and to allow the recovery of the NAMI A/ferritin adducts. Electronic spectra were repeated on the filtered and on the flow-through fractions highlighting a new relatively broad transition in the HuHf sample at *ca.* 500 nm, not referable to NAMI A or to the protein, suggesting that a chromophoric ruthenium centre is now bound to the protein (Fig. 3).

In order to characterize more in depth the final NAMI A/HuHf adducts, we collected circular dichroism spectra on protein samples treated with increasing amounts of the complex. Analysis of the far UV spectra showed only slight differences between the apo and holo (treated with NAMI A) forms of HuHf, confirming the maintenance of the secondary structure after ruthenium binding (Fig. 4A). However, the CD spectra in the 300–700 nm region exhibited two bands: the first one is positive and centered at 360 nm with a shoulder around 420 nm; the second one, centered at *ca.* 500 nm, is negative (Fig. 4B). The observation of a negative dichroic band in the visible region at *ca.* 500 nm is diagnostic for the presence of a chiral Ru center bound to HuHf. A similar CD behavior was previously reported in the case of NAMI A/BSA adducts.[44]

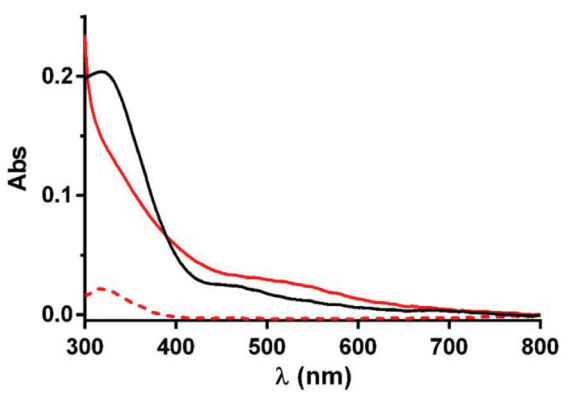

Fig. 3 Electronic spectra of ultra-filtered NAMI A/HuHf sample after 24 h of incubation. The curves referring to NAMI A/HuHf are shown in red. The spectrum of the filtered sample is reported as a continuous line, whereas that of the flow-through fraction is reported as a dotted line. The 24 h spectrum of NAMI A alone is shown in black as the reference. HuHf concentration: 50 μM in subunits; NAMI A concentration: 100 μM.

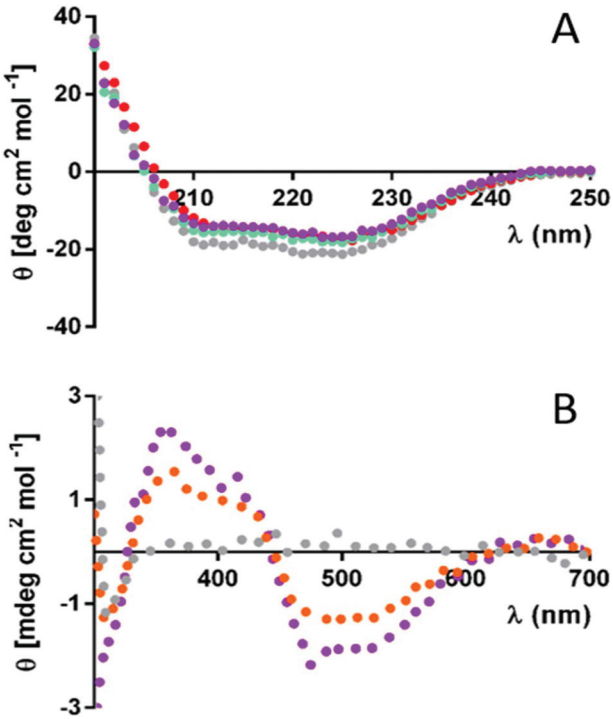

Fig. 4 CD spectra of apo HuHf and of the protein incubated for 24 h with increasing amounts of NAMI A. (A) Far UV CD spectra of apo HuHf (grey dots) and of the protein in the presence of 2, 4 and 8 equivalents of NAMI A per subunit (violet, cyan and red dots, respectively). (B) CD analysis in the 300–700 nm region of apo HuHf (grey points) and with 1 and 2 equivalents of NAMI A per subunit (orange and violet dots, respectively). In this case, due to the high protein concentration (millimolar range) needed to register the CD spectra, precipitation and aggregation phenomena prevented the characterization of samples at a metal : protein ratio higher than 4.

To quantify the amount of Ru bound to the protein, ICP-AES determinations of the various fractions were performed (Fig. 5). NAMI A/HuHf samples (with initial 2 : 1, 4 : 1 and 8 : 1 metal to protein subunit ratios) showed an increasing amount of bound ruthenium atoms per ferritin subunit: 0.61 : 1 (2 : 1), 0.94 : 1 (4 : 1) and 1.21 : 1 (8 : 1). However, it is interesting to note that even upon exposure to an 8-fold excess of NAMI A, the final stoichiometry was only slightly greater than 1 Ru mole per ferritin subunit, suggesting the presence of only a single ruthenium binding site per subunit.

X-ray crystallography

The structure of the NAMI A/HuHf adduct was solved at 1.58 Å resolution (Fig. 6). All the atoms of residues 4–176 of HuHf in the adduct nicely fit into the final 2Fo–Fc electron density map. The structure of the protein in the adduct is very similar to that of the ruthenium-free protein used as the starting model: HuHf adopts the four-helix bundle structure typical of the ferritin fold. Superposition of a single chain of NAMI A/HuHf to that of native HuHf gives an r.m.s.d. of 0.10 Å between Cα atoms.

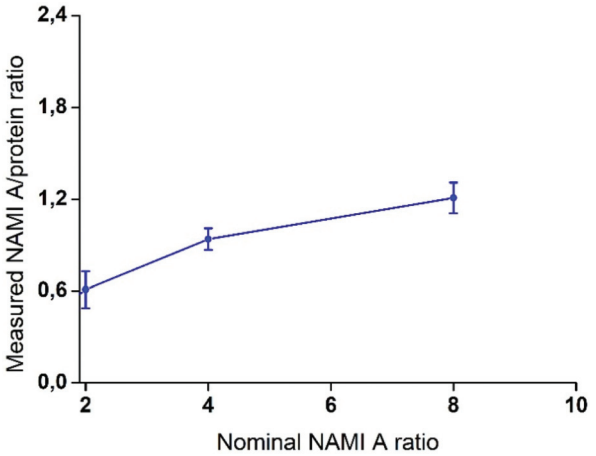

Fig. 5 ICP-AES data of ruthenium bound to HuHf subunit *vs.* nominal NAMI A/protein ratio. Each point was obtained from the average of three different ICP-AES measurements.

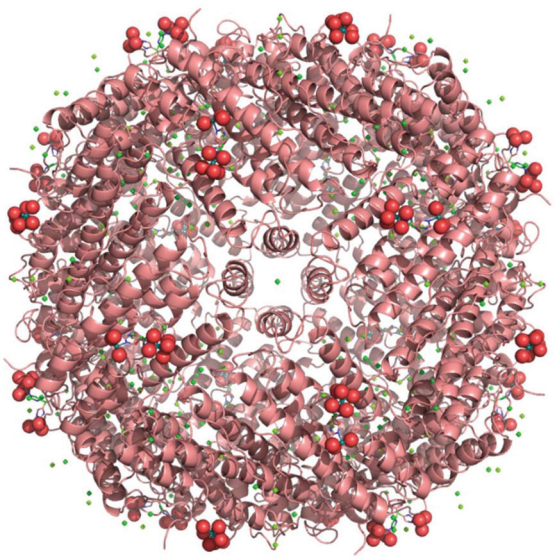

Fig. 6 Ribbon representation of the overall structure of the NAMI A/HuHf adduct. The side chain of His105 is shown in ball and stick, while Ru and water molecules completing the metal coordination sphere are shown as spheres.

The 2Fo–Fc electron density map of the Ru-binding site in the NAMI A/HuHf adduct is shown in Fig. 7. A Ru ion from NAMI A binds the side chain of His105 onto the external surface of each subunit, with water molecules completing the distorted octahedral coordination sphere of the metal. His105 adopts two distinct conformations with the Ru centre occupying two alternative positions (Fig. 7) that were refined with occupancy factors equal to 0.25 and 0.35, respectively. *B*-Factors of residues and water molecules surrounding the Ru centres are reported in Table S1 of the ESI.† In one of these two Ru-containing fragments, two metal ligands were not added to the final model, due to the absence of a clear electron density map, but

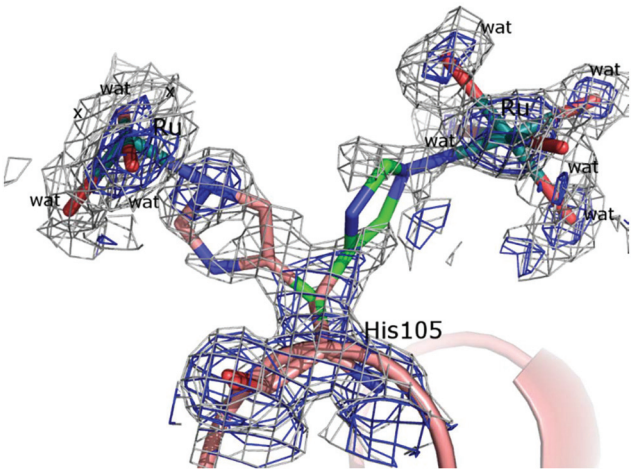

Fig. 7 2Fo–Fc electron density, calculated after the final refinement run (contoured at 0.5 and 1σ levels and reported in blue and grey, respectively), at the Ru binding site. His105 adopts two different conformations that are depicted in green and pink, respectively. X indicates missing ligands. For a comparison with the electron density map close to the His105 side chain in native HuHf, see Fig. S5B and S5C in the ESI of ref. 28.

this is not surprising considering the low occupancy of the Ru centre at this site. The presence of alternate conformations of the ruthenated His105 side chain is associated with that of the side chains of Lys108, Asn109, Cys102, Gln112 and Arg156 that are in close proximity to the Ru binding site. The intricate network of hydrogen bonds that are formed between residues that line this region and water molecules is reported in Fig. 8.

These results agree with our previous data on the structures of the major products of the reaction of lysozyme[45] and carbonic anhydrase[46] with NAMI A: NAMI A completely degrades upon protein binding and loses all its original ligands; even-

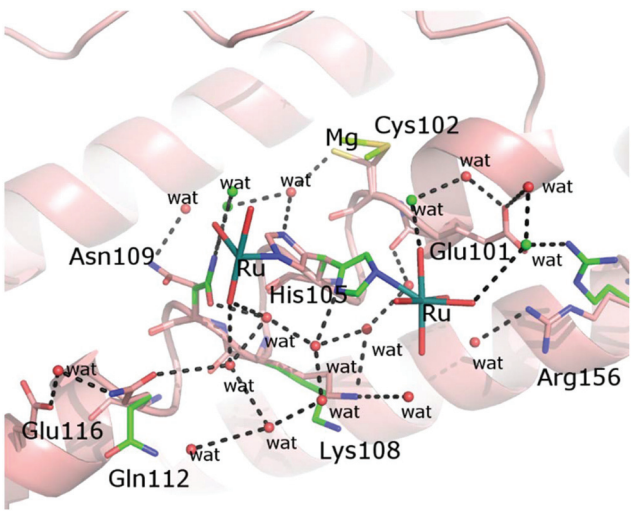

Fig. 8 Hydrogen bonds formed in close proximity of the Ru binding site. The two alternative conformations of the His105 side chain are coloured in pink and green, respectively. Water molecules associated exclusively with the latter conformation are shown in green.

tually, naked Ru ions bind residue side chains on the surface of the protein.[47] Interestingly, His105 was already identified as one of the metal binding sites in the adduct that HuHf forms with cisplatin.[28]

The structure of the NAMI A/HuHf adduct will be hereafter denoted as "ruthenated" HuHf.

Inhibition of the ferroxidase activity in HuHf

In order to evaluate whether Ru-metalation may affect the uptake and oxidation of iron ions, HuHf was incubated for 24 h with NAMI A at 1 : 2 molar ratio (HuHf 100 μM in subunits) and the kinetics of the iron oxidation of ruthenated ferritin (after removal of unreacted Ru species) was monitored using stopped-flow spectrophotometry. Kinetic measurements were performed at two different wavelengths. A maximum absorption at 650 nm is characteristic of diferric-peroxo (DFP) formation. DFP is the first transient intermediate that forms at the catalytic site during iron(II) oxidation. Afterwards, DFP decays rapidly to diferric-oxo complexes, DFO(H), that represent the precursor of the ferric biomineral that grows in the cavity.

The DFO(H) species, and DFP, show a general absorption at 350 nm.[48] The initial rates of the formation of DFP ($A_{650\ nm}$) and DFO(H) ($A_{350\ nm}$) for native and ruthenated HuHf (protein preincubated with NAMI A; Table 2) were calculated taking into account the changes in absorbance in the first milliseconds of the traces at 650 nm and 350 nm (Fig. 9). Remarkably, we observed a partial inhibition of the ferroxidase activity in the case of the ruthenated protein, both in the formation of ferric oxo species and DFP (Table 2).

Table 2 Catalytic reaction rates. Initial rates of formation for DFP ($\Delta A_{650\ nm}/\Delta t$) and for DFO(H) species ($\Delta A_{350\ nm}/\Delta t$) are shown as mean values from two independent analysis with SEM (standard error of the mean). For each analysis, the percentage of inhibition of the ruthenated protein with respect to the apo form is reported

	HuHf	Ruthenated HuHf	Activity inhibition (%)
$\Delta A_{650\ nm}/\Delta t$	1.414 ± 0.011	1.262 ± 0.034	10
$\Delta A_{350\ nm}/\Delta t$	1.998 ± 0.099	1.578 ± 0.027	20

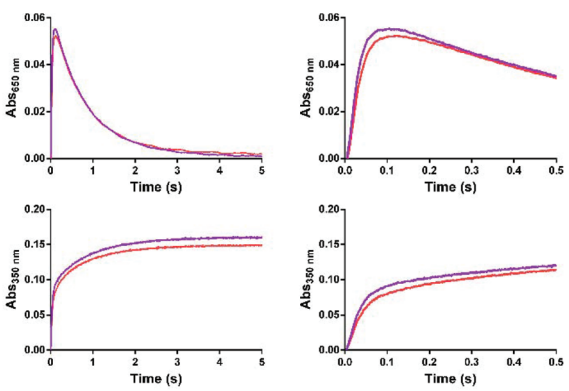

Fig. 9 Kinetics of product formation in HuHf (purple curves) and ruthenated HuHf (red curves). Reaction progress of DFP ($Abs_{650\ nm}$) and DFO (H) ($Abs_{350\ nm}$) formation measured using stopped-flow spectrophotometry (mean ± SEM). The panels on the left represent the plots of the changes in absorbance for 5 seconds, while the panels on the right show an enlargement of 0.5 seconds of the reaction to highlight the differences in the initial rates.

Conclusions

In this study, we have investigated in depth the interactions occurring between the experimental anticancer drug NAMI A and human H-chain ferritin, the main goal being the preparation and characterisation of NAMI A/ferritin adducts possibly showing better pharmacological properties and an improved drug delivery performance. Spectroscopic analysis of the NAMI A/HuHf system revealed that the presence of ferritin does not affect dramatically the characteristic hydrolysis pattern of NAMI A in physiological media, even though an appreciable increase in the rate of NAMI A hydrolysis was detected. On the other hand, spectral studies revealed that the reaction of NAMI A with HuHf results in the formation of an adduct with characteristic absorption and circular dichroic spectral features in the visible region. Notably, a series of ICP-AES determinations pointed out the predominant formation of a 1 : 1 Ru/HuHf subunit adduct. Indeed, though exposed to relatively large quantities of NAMI A (up to 8 : 1), the maximum amount of protein bound ruthenium that we could measure was only 1.26 Ru atoms per monomeric unit.

The X-ray structure of the above NAMI A/HuHf adduct was eventually solved at 1.58 Å resolution, allowing clear identification of the Ru binding site. The ruthenium ion, coordinated to five water molecules with its typical octahedral geometry, binds the side chain of His105, a surface exposed residue. The nature of NAMI A binding to HuHf closely reproduces the behaviour previously reported for lysozyme[45] and human carbonic anhydrase II,[46] where only a naked ruthenium ion is eventually bound to the protein at an exposed His residue, whereas all the other original Ru ligands are released. On the other hand, kinetic measurements showed that ruthenated HuHf has a slightly lower ferroxidase activity compared to the native form; in any case, complete suppression of the enzymatic activity was not observed in accord with the fact that ruthenium binds far apart from the catalytic centre. This NAMI A/HuHf adduct is of potential pharmaceutical interest as a selective carrier of ruthenium ions to cancer tissues and its pharmacological profile will be investigated soon in suitable cellular models.

Conflicts of interest

There are no conflicts to declare.

Acknowledgements

L. M. thanks Beneficentia Stiftung, ITT (Istituto Toscano Tumori), Ente Cassa Risparmio Firenze (ECR) and AIRC (IG-16049) for their financial support. The CIRCMSB consor-

tium is also acknowledged. A. M. and G. F. thank M. Caterino and the ESRF staff for technical assistance.

Notes and references

1 E. S. Antonarakis and A. Emadi, *Cancer Chemother. Pharmacol.*, 2010, **66**, 1–9.
2 G. Tamasi, A. Carpini, D. Valensin, L. Messori, A. Pratesi, F. Scaletti, M. Jakupec, B. Keppler and R. Cini, *Polyhedron*, 2014, **81**, 227–237.
3 E. Alessio, *Eur. J. Inorg. Chem.*, 2017, **12**, 1549–1560.
4 E. Alessio and L. Messori, *Met. Ions Life Sci.*, 2018, **18**, 141–170.
5 L. Biancalana, A. Pratesi, F. Chiellini, S. Zacchini, T. Funaioli, C. Gabbiani and F. Marchetti, *New J. Chem.*, 2017, **41**, 14574–14588.
6 A. Bergamo, T. Riedel, P. J. Dyson and G. Sava, *Invest. New Drugs*, 2015, **33**, 53–63.
7 M. Bacac, M. Vadori, G. Sava and S. Pacor, *Cancer Immunol. Immunother.*, 2004, **53**, 1101–1110.
8 S. Leijen, S. A. Burgers, P. Baas, D. Pluim, M. Tibben, E. van Werkhoven, E. Alessio, G. Sava, J. H. Beijnen and J. H. M. Schellens, *Invest. New Drugs*, 2015, **33**, 201–214.
9 J. Wang and K. Pantopoulos, *Biochem. J.*, 2011, **434**, 365–381.
10 E. L. Mackenzie, K. Iwasaki and Y. Tsuji, *Antioxid. Redox Signaling*, 2008, **10**, 997–1030.
11 S. C. Andrews, P. Arosio, W. Bottke, J. F. Briat, M. Vondarl, P. M. Harrison, J. P. Laulhere, S. Levi, S. Lobreaux and S. J. Yewdall, *J. Inorg. Biochem.*, 1992, **47**, 161–174.
12 C. Pozzi, S. Ciambellotti, C. Bernacchioni, F. Di Pisa, S. Mangani and P. Turano, *Proc. Natl. Acad. Sci. U. S. A.*, 2017, **114**, 2580–2585.
13 M. Uchida, S. Kang, C. Reichhardt, K. Harlen and T. Douglas, *Biochim. Biophys. Acta*, 2010, **1800**, 834–845.
14 L. Li, C. Fang, J. C. Ryan, E. C. Niemi, J. A. Lebrón, P. J. Björkman, H. Arase, F. M. Torti, S. V. Torti, M. C. Nakamura and W. E. Seaman, *Proc. Natl. Acad. Sci. U. S. A.*, 2010, **107**, 3505–3510.
15 J. Yi Li, N. Paragas, R. M. Ned, A. Qiu, M. Viltard, T. Leete, I. R. Drexler, X. Chen, S. Sanna-Cherchi, F. Mohammed, D. Williams, C. Sheng Lin, K. M. Schmidt-Ott, N. C. Andrews and J. Barasch, *Dev. Cell*, 2009, **16**, 35–46.
16 D. Hogemann-Savellano, E. Bos, C. Blondet, F. Sato, T. Abe, L. Josephson, R. Weissleder, J. Gaudet, D. Sgroi, P. J. Peters and J. P. Basilion, *Neoplasia*, 2003, **5**, 495–506.
17 L. Mendes-Jorge, D. Ramos, A. Valenca, M. Lopez-Luppo, V. M. R. Pires, J. Catita, V. Nacher, M. Navarro, A. Carretero, A. Rodriguez-Baeza and J. Ruberte, *PLoS One*, 2014, **9**, e106974.
18 X. T. Ji, L. Huang and H. Q. Huang, *J. Proteomics*, 2012, **75**, 3145–3157.
19 Z. Yang, X. Wang, H. Diao, J. Zhang, H. Li, H. Sun and Z. Guo, *Chem. Commun.*, 2007, **33**, 3453–3455.
20 N. Pontillo, F. Pane, L. Messori, A. Amoresano and A. Merlino, *Chem. Commun.*, 2016, **52**, 4136–4139.
21 N. Pontillo, G. Ferraro, J. R. Helliwell, A. Amoresano and A. Merlino, *ACS Med. Chem. Lett.*, 2017, **8**, 433–437.
22 R. M. Xing, X. Y. Wang, C. L. Zhang, Y. M. Zhang, Q. Wang, Z. Yang and Z. J. Guo, *J. Inorg. Biochem.*, 2009, **103**, 1039–1044.
23 K. Fujita, Y. Tanaka, T. Sho, S. Ozeki, S. Abe, T. Hikage, T. Kuchimaru, S. Kizaka-Kondoh and T. Ueno, *J. Am. Chem. Soc.*, 2014, **136**, 16902–16908.
24 Y. Takezawa, P. Böckmann, N. Sugi, Z. Wang, S. Abe, T. Murakami, T. Hikage, G. Erker, Y. Watanabe, S. Kitagawa and T. Ueno, *Dalton Trans.*, 2011, **40**, 2190–2195.
25 D. M. Monti, G. Ferraro, G. Petruk, L. Maiore, F. Pane, A. Amoresano, M. A. Cinellu and A. Merlino, *Dalton Trans.*, 2017, **46**, 15354–15362.
26 G. Ferraro, D. M. Monti, A. Amoresano, N. Pontillo, G. Petruk, F. Pane, M. A. Cinellu and A. Merlino, *Chem. Commun.*, 2016, **52**, 9518–9521.
27 S. Zhang, J. Zang, H. Chen, M. Li, C. Xu and G. Zhao, *Small*, 2017, **13**, 1701045.
28 G. Ferraro, S. Ciambellotti, L. Messori and A. Merlino, *Inorg. Chem.*, 2017, **56**, 9064–9070.
29 C. Pozzi, F. Di Pisa, C. Bernacchioni, S. Ciambellotti, P. Turano and S. Mangani, *Acta Crystallogr., Sect. D: Biol. Crystallogr.*, 2015, **71**, 1909–1920.
30 E. Ravera, S. Ciambellotti, L. Cerofolini, T. Martelli, T. Kozyreva, C. Bernacchioni, S. Giuntini, M. Fragai, P. Turano and C. Luchinat, *Angew. Chem., Int. Ed.*, 2016, **55**, 2446–2449.
31 G. Sava, E. Alessio, A. Bergamo and G. Mestroni, in *Topics in Biological Inorganic Chemistry*, ed. M. J. Clarke and P. J. Sadler, Springer, Berlin, 1999, pp. 143–169.
32 A. Pratesi, D. Cirri, M. D. Đurović, S. Pillozzi, G. Petroni, Ž. D. Bugarčić and L. Messori, *BioMetals*, 2016, **29**, 905–911.
33 I. Russo Krauss, G. Ferraro, A. Pica, J. Márquez, J. R. Helliwell and A. Merlino, *Metallomics*, 2017, **9**, 1534–1547.
34 T. G. G. Battye, L. Kontogiannis, O. Johnson, H. R. Powell and A. G. W. Leslie, *Acta Crystallogr., Sect. D: Biol. Crystallogr.*, 2011, **67**, 271–281.
35 A. J. McCoy, R. W. Grosse-Kunstleve, P. D. Adams, M. D. Winn, L. C. Storoni and R. J. Read, *J. Appl. Crystallogr.*, 2007, **40**, 658–674.
36 G. N. Murshudov, P. Skubák, A. A. Lebedev, N. S. Pannu, R. A. Steiner, R. A. Nicholls, M. D. Winn, F. Long and A. A. Vagin, *Acta Crystallogr., Sect. D: Biol. Crystallogr.*, 2011, **67**, 355–367.
37 P. Emsley, B. Lohkamp, W. G. Scott and K. Cowtan, *Acta Crystallogr., Sect. D: Biol. Crystallogr.*, 2010, **66**, 486–501.
38 R. A. Laskowski, M. W. MacArthur, D. S. Moss and J. M. Thornton, *J. Appl. Crystallogr.*, 1993, **26**, 283–291.
39 W. L. DeLano, *PyMOL*, 2002, http://www.pymol.org.
40 H. Berman, K. Henrick and H. Nakamura, *Nat. Struct. Biol.*, 2003, **10**, 980.

41 I. Landini, A. Lapucci, A. Pratesi, L. Massai, C. Napoli, G. Perrone, P. Pinzani, L. Messori, E. Mini and S. Nobili, *Oncotarget*, 2017, **8**, 96062–96078.
42 G. Sava, S. Pacor, G. Mestroni and E. Alessio, *Clin. Exp. Metastasis*, 1992, **10**, 273–280.
43 E. Alessio, G. Balducci, A. Lutman, G. Mestroni, M. Calligaris and W. M. Attia, *Inorg. Chim. Acta*, 1993, **203**, 205–217.
44 L. Messori, P. Orioli, D. Vullo, E. Alessio and E. Iengo, *Eur. J. Biochem.*, 2000, **267**, 1206–1213.
45 L. Messori and A. Merlino, *Dalton Trans.*, 2014, **43**, 6128–6131.
46 A. Casini, C. Temperini, C. Gabbiani, C. T. Supuran and L. Messori, *ChemMedChem*, 2010, **5**, 1989–1994.
47 A. Merlino, *Coord. Chem. Rev.*, 2016, **326**, 111–134.
48 E. C. Theil, R. K. Behera and T. Tosha, *Coord. Chem. Rev.*, 2013, **257**, 579–586.